Atmos. Chem. Phys., 15, 583–593, 2015
www.atmos-chem-phys.net/15/583/2015/
doi:10.5194/acp-15-583-2015

Atmospheric Chemistry and Physics
Open Access

Iodine oxide in the global marine boundary layer

C. Prados-Roman[1], C. A. Cuevas[1], T. Hay[1], R. P. Fernandez[1,*], A. S. Mahajan[1,], S.-J. Royer[2], M. Galí[2,***], R. Simó[2], J. Dachs[3], K. Großmann[4], D. E. Kinnison[5], J.-F. Lamarque[5], and A. Saiz-Lopez[1]**

[1]Atmospheric Chemistry and Climate Group, Institute of Physical Chemistry Rocasolano (CSIC), Madrid, Spain
[2]Institute of Marine Sciences (CSIC), Barcelona, Spain
[3]Institute of Environmental Assessment and Water Research (CSIC), Barcelona, Spain
[4]Institute of Environmental Physics, University of Heidelberg, Heidelberg, Germany
[5]Atmospheric Division, NCAR, Boulder, CO, USA
[*]now at: National Scientific and Technical Research Council (CONICET), UTN-FR Mendoza/ICB-UNCuyo, Mendoza, Argentina
[**]now at: Indian Institute of Tropical Meteorology, Pune, India
[***]now at: Takuvik (UL/CNRS), Quebec, Canada

Correspondence to: A. Saiz-Lopez (a.saiz@csic.es)

Received: 30 July 2014 – Published in Atmos. Chem. Phys. Discuss.: 29 August 2014
Revised: 4 December 2014 – Accepted: 5 December 2014 – Published: 16 January 2015

Abstract. Emitted mainly by the oceans, iodine is a halogen compound important for atmospheric chemistry due to its high ozone depletion potential and effect on the oxidizing capacity of the atmosphere. Here we present a comprehensive data set of iodine oxide (IO) measurements in the open marine boundary layer (MBL) made during the Malaspina 2010 circumnavigation. Results show IO mixing ratios ranging from 0.4 to 1 pmol mol^{-1} (30 % uncertainty) and, complemented with additional field campaigns, this data set confirms through observations the ubiquitous presence of reactive iodine chemistry in the global marine environment. We use a global model with organic (CH_3I, CH_2ICl, CH_2I_2 and CH_2IBr) and inorganic (HOI and I_2) iodine ocean emissions to investigate the contribution of the different iodine source gases to the budget of IO in the global MBL. In agreement with previous estimates, our results indicate that, globally averaged, the abiotic precursors contribute about 75 % to the IO budget. However, this work reveals a strong geographical pattern in the contribution of organic vs. inorganic precursors to reactive iodine in the global MBL.

1 Introduction

The atmospheric relevance of reactive halogens became clear decades ago when their potential to catalytically destroy ozone (O_3) was first recognised in the polar stratosphere (Molina and Rowland, 1974) and later on in the troposphere (e.g. Barrie et al., 1988). Halogens are also known to affect the NO_x (NO, NO_2) and HO_x (HO, HO_2) partitioning and the lifetime of organic compounds, to alter the sulphur and mercury cycles and, in the case of iodine oxides, to form ultrafine particles in coastal areas (Saiz-Lopez and von Glasow, 2012 and references therein).

Since the first study to deal with the tropospheric relevance of inorganic iodine (Chameides and Davis, 1980), major efforts have been made to detect reactive iodine species in their main source region: the oceans (Saiz-Lopez et al., 2012 and references therein). Several field campaigns in scattered marine environments have aimed at detecting IO – a beacon for the presence of active iodine chemistry – and determining the nature and strength of organic and inorganic source gases of iodine (referenced hereafter as OSG and ISG respectively). Air–sea fluxes of iodocarbons (CH_3I, CH_2I_2, CH_2ICl and CH_2IBr, C_2H_5I, 1-C_3H_7I, 2-C_2H_7I) have been reported (Carpenter et al., 2012) but were insufficient in general observations to explain measured IO concentrations in the marine boundary layer (MBL), implying the existence of an abiotic

Table 1. Description of the different legs of the Malaspina 2010 expedition. Due to technical problems, the O_3 and IO measurements presented in this work correspond to the period from 21 February 2011 to 12 July 2011.

Legs	Docking places	Docking dates (dd/mm/yyyy)
1	Cádiz (Spain) – Rio de Janeiro (Brazil)	14/12/2010–13/01/2011
2	Rio de Janeiro (Brazil) – Cape Town (South Africa)	17/01/2011–06/02/2011
3	Cape Town (South Africa) – Perth (Australia) – Sydney (Australia)	11/02/2011–13/03/2011–30/03/2011
4	Sydney (Australia) – Auckland (New Zealand) – Honolulu (Hawaii)	04/04/2011–13/04/2011–08/05/2011
5	Honolulu (Hawaii) – Panama (Panama) – Cartagena de Indias (Colombia)	13/05/2011–10/06/2011–13/06/2011
6	Cartagena de Indias (Colombia) – Cartagena (Spain)	19/06/2011–14/07/2011

ocean source of iodine (Mahajan et al., 2010, 2012; Jones et al., 2010; Gómez Martín et al., 2013a; Großmann et al., 2013; Lawler et al., 2014). In several one-dimensional model studies, simulated emissions of molecular iodine (I_2) were used to fit IO observations (e.g. Mahajan et al., 2010; Großmann et al., 2013); however, the recent work of Lawler et al. (2014) with the first observation of I_2 in the remote MBL confirmed that the emission of I_2 is still insufficient to explain the observed levels of IO. Recently, the study of Carpenter et al. (2013) has experimentally confirmed that not only I_2 is emitted naturally from the oceans but also, and mainly, hypoiodous acid (HOI). In that study and in the subsequent work of MacDonald et al. (2014), the authors have confirmed through laboratory work that the oceanic emission of ISG (HOI and I_2) follows the deposition of tropospheric O_3 to the oceans and its reaction with aqueous iodide (I^-_{aq}, Garland et al., 1980), and they proposed a parameterisation for ocean ISG emissions dependent on O_3, wind speed (ws) and sea surface temperature (SST).

In this work, we present a comprehensive map of IO observations in the global MBL showing the ubiquity of this radical in the marine environment. Moreover, by means of a global model including OSG and ISG oceanic emissions, we investigate the geographical emission patterns of both iodine precursors and their contribution to the IO budget in the marine environment. Section 2 details the measurement campaign of Malaspina 2010 and provides information on the chemical model used throughout this work. Section 3 presents the results of the IO observations and the modelling studies, and Sect. 4 concludes this work.

2 Measurements and model

In the following we present the setup of the O_3 and IO measurements during the Malaspina 2010 expedition as well as the model schemes used in this study.

2.1 Measurements during the Malaspina 2010 circumnavigation

From December 2010 until July 2011 the Spanish research vessel Hesperides circumnavigated the world's oceans within the framework of the Malaspina 2010 project. The main objectives of this interdisciplinary campaign were to investigate the biogeochemistry, physical properties and microbiological biodiversity of the oceans; the genetic diversity of the deep ocean and the exchange of trace gases and pollutants with the atmosphere; and the impact of global change in the ocean. The different legs of the cruise and the docking dates are indicated in Table 1.

A multi-axis differential optical absorption spectroscopy instrument (MAX-DOAS; Platt and Stutz, 2008) and a commercial 2B-205 ozone monitor, along with a GPS, were deployed aboard the vessel in order to investigate the presence of atmospheric trace gases such as IO, O_3, BrO, HCHO and CHOCHO in the MBL. Herein we focus on the observations of IO and O_3 during the campaign.

2.1.1 Surface ozone

The ozone monitor was installed in the ship's bridge with a 5 m long Teflon-lined inlet tube from the upper deck, well forward of the exhaust stacks (∼15 m a.s.l.). The inlet was placed just above the railing in the air coming from the front of the ship, avoiding sampling air from the ship's boundary layer. Due to GPS communication errors, our data compilation started on 21 February 2011 (second leg) and finished on 12 July 2011.

The ozone volume mixing ratios (vmr) observed during Malaspina 2010 are presented in Fig. 1a along with the ancillary measurements of relevance for the present work (i.e. SST and ws; Fig. 1 and Table 2). Simulations of the 5 day backward trajectories of the air masses arriving at the ship's track are provided in Fig. 2, showing the typical non-continental origin of the air masses sensed during the cruise.

2.1.2 Iodine oxide

Aiming at the detection of IO along the track of the Malaspina expedition, a MAX-DOAS instrument was installed on the second deck near the rear of the ship (∼10 m a.s.l.). Briefly, these instruments measure the intensity of scattered light in the UV–VIS range entering a scanning telescope at several precise viewing angles and have been widely used for atmospheric composition research

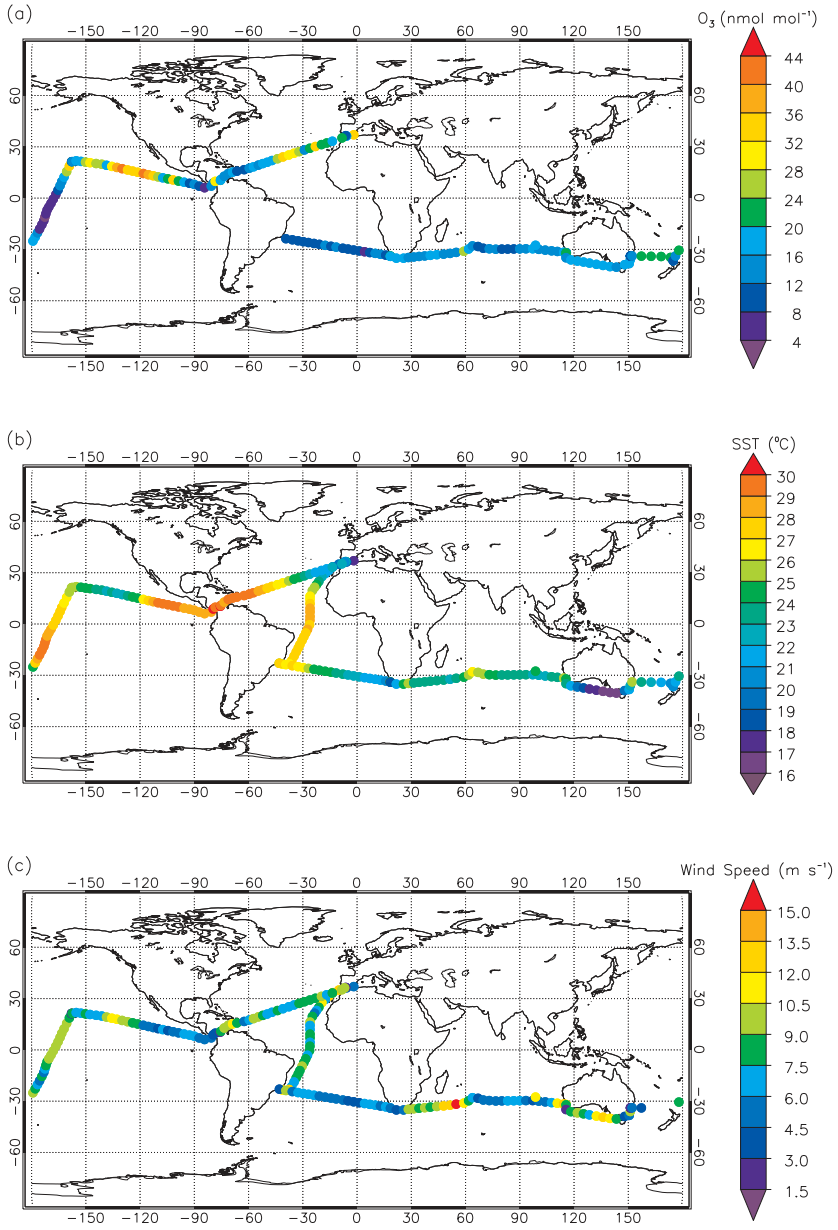

Figure 1. Observations of surface ozone and ancillary parameters during Malaspina 2010 (daily average): **(a)** O_3 mixing ratios, **(b)** sea surface temperature and **(c)** wind speed; see also Table 2.

Table 2. Summary of the O_3 and ancillary parameters measured during Malaspina 2010. The data correspond to daytime average values concurrent with the IO measurements gathered during the expedition (Fig. 1).

Parameter	Mean	SD	Minimum	Maximum
O_3 (nmol mol^{-1})	16.0	9.4	3.4	42.4
ws (m s^{-1})	7.0	2.0	3.3	11.6
SST (K)	298.9	2.9	291.6	303.0

(Platt and Stutz, 2008). Thus only a summary of the particular MAX-DOAS instrument mounted on the Hesperides research vessel is given hereafter. For details regarding the MAX-DOAS technique, please refer to the work of, e.g., Platt and Stutz (2008) and Hönninger et al. (2004); for further details of our ship-based MAX-DOAS instrument, please see Mahajan et al. (2012).

Briefly explained, in the case of the Malaspina's MAX-DOAS instrument, the scanning telescope was housed in a weatherproof metal chamber with a flat UV-transmitting acrylic window and a sunshade to reduce spectral effects on

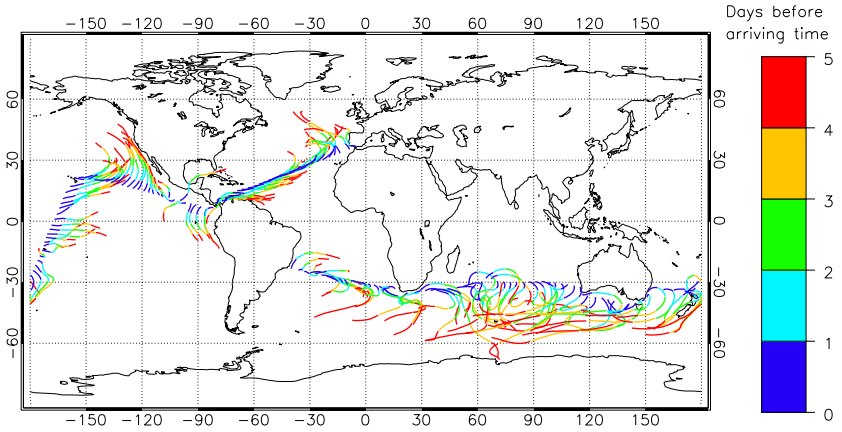

Figure 2. Backward trajectories of the air masses arriving at noon on every day of the Malaspina expedition. They were calculated using HYbrid Single-Particle Lagrangian Integrated Trajectory (HYSPLIT; Draxler and Rolph, 2014).

the window. The telescope unit (built by the New Zealander National Institute of Water and Atmospheric Research, or NIWA) was mounted on a gimbal table to compensate for the pitch and roll of the ship. The gimbal dampened the effective oscillations in telescope elevation angle to $\pm 1°$ for most of the cruise and $\pm 2°$ in rough conditions. In addition, a high accuracy ($\pm 0.1°$), fast response (0.3 s) inclinometer was used to log the residual oscillations in order to correct the elevation angles. Only true angles within 0.2° of each prescribed elevation angle were used for analysis. The azimuth viewing direction was towards the ship's bow (20° anticlockwise) to minimise exhaust emissions in the line of sight. The scanning telescope consisted of a rotating diagonal mirror driven by a stepper motor and a 50.8 mm diameter fused silica lens with a focal length of 200 mm, giving a field of view of 0.5°. The light was focused onto a 5 m long 19 optic fibre bundle leading to a Princeton Instruments SP500i spectrometer with a Princeton Instruments Pixis 400B CCD camera. A 600 grooves mm^{-1} grating was used, giving approximately an 80 nm spectral window and a spectral resolution of 0.5 nm FWHM. Spectra were recorded for a short exposure time of 1 s at each discrete elevation angle (2, 4, 6, 8, 10, 15, 30 and 90°) in order to minimise potential deviations in angle due to the ship's movement. The scan sequence was repeated every 2 min and after every 10 cycle the grating was shifted between the two wavelength regions, centred on 358 nm (UV spectral range) and 440 nm (VIS spectral range). Results presented in this work correspond to the VIS channel, where IO could be measured (see Sect. 3.1).

2.2 Modelling the oceanic emissions of reactive iodine precursors

We implemented the experimentally derived ocean fluxes of ISG (Carpenter et al., 2013; MacDonald et al., 2014) into the global chemistry–climate model CAM-Chem (Community Atmospheric Model with Chemistry, version 4.0; Lamarque et al., 2012), which already included a validated OSG emissions inventory and a state-of-the-art halogen chemistry scheme (Ordónez et al., 2012). The on-line ISG flux formulation, based on the studies of Carpenter et al. (2013) and MacDonald et al. (2014), was performed considering the instantaneous modelled levels of surface O_3, SST and ws in each of the model grid boxes over the oceans (i.e. imposing an ocean mask). In the following we summarise the model schemes used in this work. Further details on the particular implementation of the ISG parameterisation into the CAM-Chem model are given in Prados-Roman et al. (2014), whereas the general model setup is described in the study of Lamarque et al. (2012).

2.2.1 Model schemes

Throughout this work, two different pairs of simulations were performed in order to evaluate the model, to identify the contribution of OSG/ISG fluxes and to estimate the iodine burden of the MBL. A brief description of the simulations used in this study is given below.

1. *Base–organic runs:* in the *base run*, simulations were performed considering the oceanic emission of organic and inorganic iodine precursors. Based on previous publications, the OSG inventory of very short-lived iodocarbons (OSG = CH_3I, CH_2I_2, CH_2IBr and CH_2ICl) was considered (Ordónez et al., 2012), while the ISG computation of HOI and I_2 was used as described in the study of Prados-Roman et al. (2014). In order to distinguish the contribution of the inorganic and the organic iodine source gases to the IO budget in the MBL, the *organic* scheme included only the above-mentioned OSG (by forcing the inorganic emissions to be null). Hence, the contribution of ISG to the IO budget in the MBL (i.e. IO_{ISG}) was defined as the difference between the IO vmr obtained in the MBL after the *base run* ($IO = IO_{ISG+OSG}$) and the IO vmr obtained after the *or-*

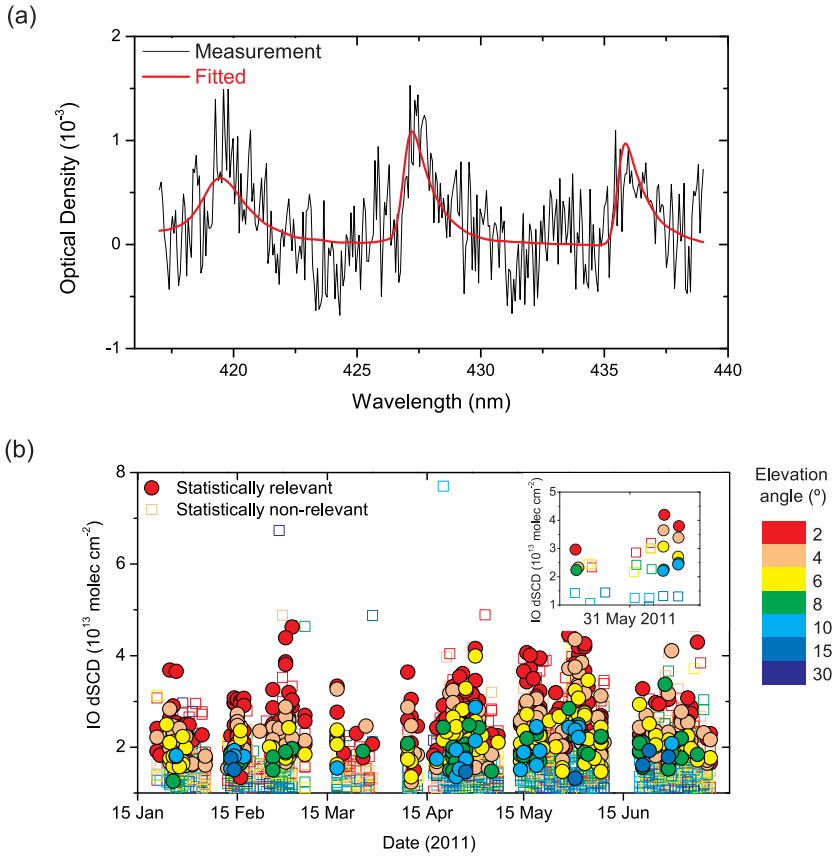

Figure 3. Retrieval of IO during the Malaspina 2010 circumnavigation. **(a)** Example of a typical IO spectral fit during the expedition. The particular spectrum was taken on 31 May 2011 (15:00 LT, 53° SZA) in the eastern Pacific for a 2° elevation angle. The black line represents the measured IO optical density and the red line represents the fitted IO after the DOAS retrieval. This fit resulted in an IO dSCD of $(3.8 \pm 0.3) \times 10^{13}$ molecules cm^{-2} (i.e. IO vmr of 0.8 ± 0.1 pmol mol^{-1}) with a residual optical density of 3.9×10^{-4} (root mean square). **(b)** Timeline of the IO dSCD observed during the expedition. Statistically relevant data (i.e. data above the quality filters; see the Supplement) are shown with filled circles and the non-relevant data with empty squares. The inset shows the daily evolution of IO dSCD for 31 May 2011. The colour code indicates the elevation angle of the measurements.

ganic run (i.e. IO_{OSG}). That is, $IO_{ISG} = (IO) - (IO_{OSG})$; the relative contribution of ISG to IO was defined as $(IO_{ISG}) / (IO)$ in percentage. Similarly, the contribution of each individual iodocarbon to the budget of IO was investigated.

2. *No phot–phot runs:* it is known that the self-reaction of IO in pristine conditions yields the formation of higher oxides (I_2O_x, $x = 2$, 3 or 4). However, once formed, the reaction pathways of these compounds are still not well understood. One possible reaction pathway is their nucleation into ultra-fine particles as observed in coastal areas (Gómez Martín et al., 2013b). Those conditions were, however, not representative of the Malaspina expedition since most of the marine atmosphere crossed was representative of an open ocean environment. A possible pathway for Malaspina's conditions was the photodissociation of those I_2O_x into OIO + I, OIO + IO or OIO + OIO as previously modelled for the Antarctic (Saiz-Lopez et al., 2008) and global marine troposphere (Saiz-Lopez et al., 2014), which would therefore result in additional reactive iodine in the MBL. The so-called *phot run* included I_2O_x photolysis while the simulation excluding such photolysis was referred to as a *no phot run*. Note that, unless stated otherwise, in the aforementioned *base–organic* schemes the I_2O_x were not allowed to photolyse but, once formed, they were lost by thermal decomposition or to pre-existing aerosols instead.

All simulations were performed with a horizontal grid resolution of 1.9° (latitude) × 2.5° (longitude) and 26 hybrid vertical levels (0–40 km) and considered the SST and sea ice boundary conditions representative of the year 2000 (Rayner et al., 2003). Note that, since the model was not run with specified dynamics, simulations are not representative of the meteorology of any specific year. Thus, unless stated otherwise, the model results presented in this work correspond to 24 h annual averages.

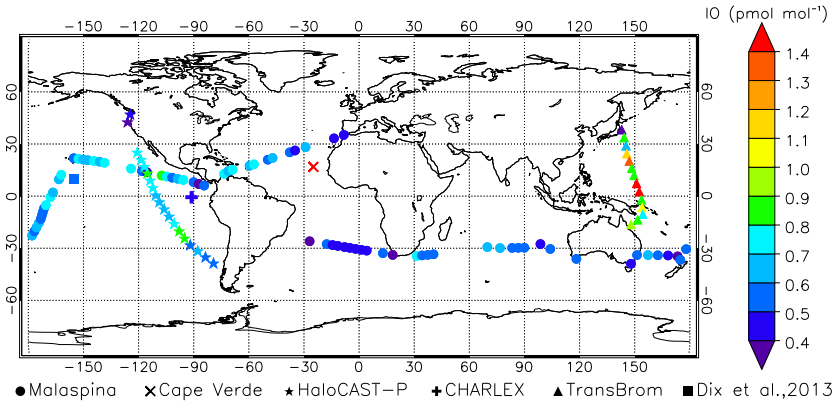

Figure 4. Iodine oxide observations in the global marine boundary layer. IO mixing ratios (in pmol mol^{-1}) are shown for five different field campaigns: Malaspina (this work), CHARLEX (Gómez Martín et al., 2013a), TransBrom (Großmann et al., 2013), HaloCAST-P (Mahajan et al., 2012) and Cape Verde (Read et al., 2008; Mahajan et al., 2010), as well as also for the MBL measurements reported by Dix et al. (2013) during one research flight. For the three ship campaigns (Malaspina, HaloCAST-P and TransBrom) daytime averaged values are shown. For the long-term measurements on the Galapagos and the Cape Verde Islands (referred to as CHARLEX and Cape Verde respectively), the mean daytime IO values observed throughout the campaigns are given.

3 Results and discussions

In this section we present the observations of IO in the MBL and compare them to different model runs. Furthermore, we investigate the contribution of the OSG and ISG fluxes to the IO budget in the MBL.

3.1 Observations of IO in the global marine boundary layer

During Malaspina 2010, IO was detected above instrumental detection limit (1.2–3.5 $\times$ 10^{13} molec cm^{-2}) in all marine environments sampled. Figure 3 shows a typical IO spectral fit during that expedition and the IO differential slant column densities (dSCD) measured along the cruise track. Note that diverse filters were used in this data set for quality assurance (e.g. cloud and wind direction filters). Following previous studies and using only IO dSCD above the quality filters, the IO mixing ratios were inferred by the well-established "O_4 method" (Wagner et al., 2004) after validating results of several days with a radiative transfer model (RTM) (e.g. Mahajan et al., 2012; Gómez Martín et al., 2013a). Particular details on these procedures (IO spectral and vmr retrieval) as well as the quality filters applied are provided in the Supplement.

Overall, during the Malaspina expedition the IO radical was constantly observed in the daytime MBL over three oceans and both hemispheres. The IO vmr integrated in the MBL ranged between 0.4 and 1 pmol mol^{-1} (detection limit of $\sim$0.2 pmol mol^{-1}), with lower values measured over the south Atlantic waters and the highest levels in the marine region west of Mexico. Figure 4 shows the averaged daytime IO vmr of the Malaspina data set, along with IO vmr obtained from former field campaigns: Cape Verde (Read et al., 2008; Mahajan et al., 2010), HaloCAST-P (Mahajan et al., 2012), CHARLEX (Gómez Martín et al., 2013a) and TransBrom (Großmann et al., 2013), as well as the value measured in the MBL by Dix et al. (2013) during a research flight. Note that the IO vmr reported for each of these campaigns are by definition intrinsically linked to the specific viewing geometry of each DOAS instrument (Platt and Stutz, 2008). During the Cape Verde campaign a long-path DOAS instrument was used with a fixed light path at 10 m a.s.l. (Read et al., 2008; Mahajan et al., 2010). In all the other campaigns shown in Fig. 4, MAX-DOAS instruments were employed. Given the different viewing elevation angles and instrumental setup, each of those MAX-DOAS instruments sensed a different part of the MBL (Platt and Stutz, 2008; Hönninger et al., 2004; Wagner et al., 2004). Although sensitivity RTM studies performed during each of those MAX-DOAS campaigns agreed on a decreasing vertical profile of IO in the MBL, the generally poor information content of the measurements hindered the vertical resolution of the inferred IO vmr vertical profiles and the reported vmr were therefore linked to a given sensed layer: particularly 0–200 m during HaloCAST-P and TransBrom (Mahajan et al., 2012; Großmann et al., 2013), 0–1200 m during CHARLEX (Gómez Martín et al., 2013a), 0–800 m during the research flight (Dix et al., 2013) and 0–600 m during Malaspina (this work, in the Supplement). Therefore the values reported in Fig. 4 should be considered as the mean IO vmr in each of the aforementioned altitude ranges linked to a given elevation angle (e.g. 2° in the case of Malaspina). Note that, despite these unavoidable retrieval limitations, Fig. 4 proves the ubiquity of IO in the global MBL and hence the presence of reactive iodine chemistry in all sub-polar marine environments.

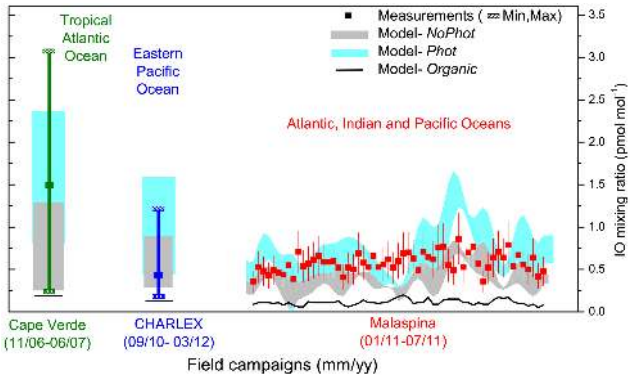

Figure 5. Measured and modelled IO mixing ratios in different field campaigns and oceans. For the two long-term campaigns on islands (Cape Verde in green and CHARLEX in blue), the mean daytime IO mixing ratio observed during the whole campaign period is given (filled squares) together with the minimum and maximum observed values (dashed rectangles) (Read et al., 2008; Mahajan et al., 2010; Jones et al., 2010). In the case of the Malaspina circumnavigation (in red), daytime averaged IO mixing ratios are provided (filled squares) along with their error (see also the Supplement). The shaded areas represent the standard deviation of the modelled fields for the *no phot* (gray) and *phot* (cyan) *base* scheme. For comparison purposes, the IO vmr modelled considering only the organic iodine precursors (*organic* run) are also included (solid black line).

3.2 Observations vs. model

Figure 4 shows the most comprehensive map of IO observations in the remote marine environment. We now use these observations together with the CAM-Chem model to evaluate the geographical distribution of IO in the MBL. The performance of the model was evaluated by comparing modelled and observed IO mixing ratios in the MBL for the aforementioned particular altitude range sensed during each campaign. Note that, as mentioned above, a key parameter in the model setup is the flux of ISG, which depends mainly on O_3 and ws (Carpenter et al., 2013; MacDonald et al., 2014). Hence, even though Fig. 4 shows IO measurements from six different field campaigns, surface O_3, ws and IO were not measured simultaneously in all of them. Thus, only the campaigns of Malaspina, CHARLEX and Cape Verde were chosen for comparison with the model. Figure 5 presents this comparison exercise, where the IO vmr observations in three oceans and both hemispheres are juxtaposed to the model output after the *organic* scheme and after the *base* run considering the *no phot* and the *phot* schemes. For this exercise the model was sampled at the same time (month) of the year and geolocation as the measurements (considering the model grid resolution of 1.9° latitude × 2.5° longitude). Note that the low IO vmr resulting after the *organic* run remains basically unaltered despite the photolysis scheme considered. Thus for simplicity only the *organic–no phot* output (i.e. *organic* run) is shown in Fig. 5.

Considering the ISG emissions along with OSG, the model reproduces satisfactorily the IO observations (Fig. 5). Note that, as found in the *organic* run, the emission of OSG alone explains on average only ∼25 % of the IO levels observed over the different oceans, a percentage that agrees well with previous one-dimensional model studies performed at specific marine environments (Mahajan et al., 2010, 2012; Jones et al., 2010; Gómez Martín et al., 2013a; Großmann et al., 2013; Lawler et al., 2014). This result points out the importance of including ISG emissions in global models. Regarding the *base* run results, the *no phot* run generally reproduces the observations, although in some regions the *phot* scheme is closer to the measurements (Fig. 5). Note that the modelled IO vmr in the *phot* scheme – likely to be a more realistic scheme for I_2O_x (Saiz-Lopez et al., 2014) – can even double the IO vmr given by the *no phot* scheme, stressing the need for further efforts from the community to investigate the fate of these higher iodine oxides. However, since the photolysis rates of I_2O_x are currently subject to uncertainty (Saiz-Lopez et al., 2014), hereafter only the *no phot* scheme is considered relevant and the results are presented as lower limits.

3.3 Sources of IO in the global marine boundary layer

After analysing the consistency of modelled vs. measured IO, in this section we investigate the sensitivity of the IO levels towards the different modelled iodine precursors. Considering the OSG emission inventory (Ordóñez et al., 2012) and the ISG (Prados-Roman et al., 2014), the modelled OSG/ISG ratio allows quantifying the individual sources and total oceanic emissions of iodine to the atmosphere. Results indicate that, globally averaged, the total oceanic iodine emissions yield 2.3 Tg yr^{-1}. From these, only 17 % (0.4 Tg yr^{-1}) originate from organic sources, which are related to bacteria, microalgae, phytoplankton, etc. (Carpenter et al., 2012). On a global average, nearly half (43 %) of the organic flux derives from CH_3I, while 29 % derives from CH_2ICl, 19 % from CH_2I_2 and 9 % from CH_2IBr, although their temporal and spatial distribution varies with, e.g., the solar radiation at sea surface and the properties of the ocean mixed layer (Bell et al., 2002; Carpenter et al., 2012; Ordóñez et al., 2012). The sea–air exchange of iodine is thus driven mainly by abiotic sources. Our results indicate that, globally averaged, 1.9 Tg (I) y^{-1} (i.e. 83 % of the total oceanic iodine fluxes) are emitted to the MBL as a result of the reaction of tropospheric O_3 with I^-_{aq} in the ocean surface and that the partitioning of these ISG emissions is directed by HOI (95 % HOI, 5 % I_2; Prados-Roman et al., 2014).

Figure 6a provides the annually averaged burden of IO in the global MBL, with values ranging from less than 0.05 pmol mol^{-1} in the sub-polar waters to ∼0.9 pmol mol^{-1} above waters offshore the Baja California peninsula. Figure 6b shows the geographical pattern of the contribution of ISG to the IO budget (i.e. IO_{ISG}). The model results indicate that, globally averaged, about 75 % of the IO in the

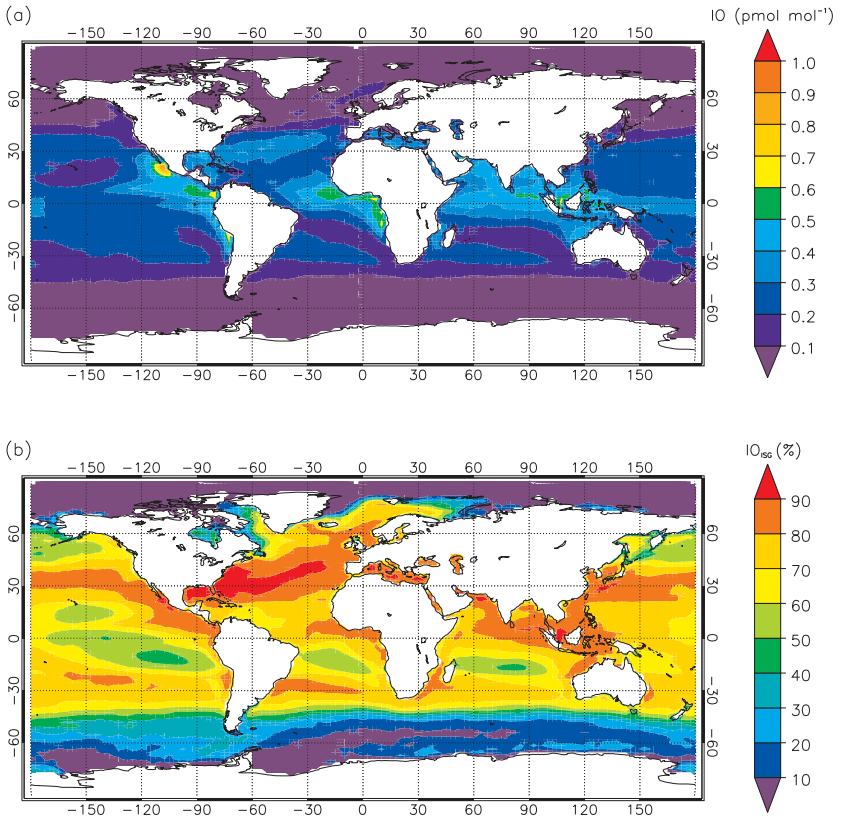

Figure 6. Simulated IO in the global marine environment (annually averaged). **(a)** Geographical distribution of the total IO budget in the MBL (i.e. $IO_{ISG+OSG}$), in units of vmr (pmol mol^{-1}). **(b)** Percentage contribution of the ISG emissions to the budget of IO in the global MBL.

MBL derives from inorganic precursors. As mentioned in the previous section, as an averaged value, this result is indeed consistent with previous estimates at given transects along the Pacific Ocean or offshore waters of Cape Verde and the Galapagos islands (Mahajan et al., 2010, 2012; Jones et al., 2010; Gómez Martín et al., 2013a; Großmann et al., 2013; Lawler et al., 2014). However, our model results show the uneven geographical distribution of IO_{ISG}: e.g. marine tropical regions in the southern hemisphere, where IO_{ISG} is of 40 %, or regions of ozone-related pollution outflow such the Bay of Bengal or the Gulf of Mexico (Myhre et al., 2013, see also the Supplement), where IO_{ISG} can be more than 90 % as a consequence of the O_3–I^-_{aq} interaction. Figure 7 shows the contribution of each of the four modelled iodocarbons to IO in the MBL, indicating that in the biological active regions of the tropics, IO derives mainly from the dihalomethanes ($CH_2ICl > CH_2I_2 > CH_2IBr$) and to a lesser extent from CH_3I. Out of those regions, CH_3I dominates the organic contribution to IO in the MBL, increasing with latitude as a result of its longer lifetime (Bell et al., 2002). Note, however, that the model simulations presented here do not include iodine emissions, organic or inorganic, from ice surfaces. Also, the strong dependence of the ISG flux with SST considerably reduces the inorganic iodine emissions over the cold waters in the high latitudes. Furthermore, as detailed in the study of MacDonald et al. (2014), the uncertainty on the parameterisation of ISG increases with decreasing SST. Thus, in the polar marine regions our simulated inorganic contribution to the IO budget should be regarded with caution. Despite these uncertainties, overall the main source of IO in the MBL at a global scale is HOI. However, as shown in Figs. 6b and 7, this is subject to strong spatial patterns in emission with regions in the southern hemisphere where the OSG can account for up to 50 % of the modelled IO levels.

4 Summary

Here we present a comprehensive set of observations of IO mixing ratios in the marine boundary layer obtained after the Malaspina 2010 circumnavigation, covering three non-polar oceans and both hemispheres. Complementing this data set with measurements gained after campaigns in the tropical Atlantic Ocean and in the eastern and western Pacific Ocean, we provide field evidence for the ubiquitous presence of IO, and thus reactive iodine chemistry, in the global marine environment. By comparing these measurements with model

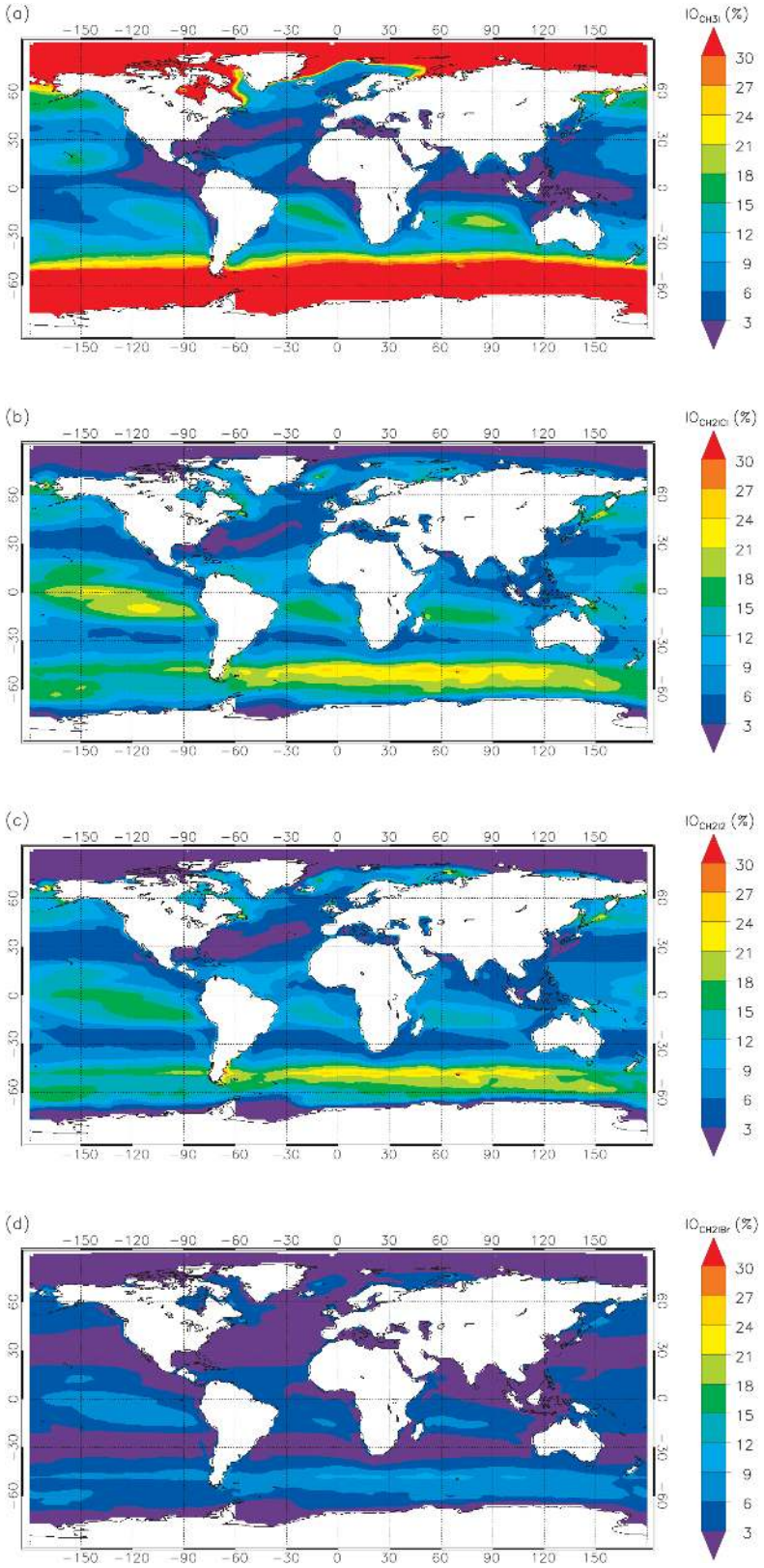

Figure 7. Simulated percentage contribution of the different short-lived iodocarbons – (**a**) CH_3I, (**b**) CH_2ICl, (**c**) CH_2I_2 and (**d**) CH_2IBr – to the IO budget in the marine environment. Note that, for comparison purposes, the colour code is the same in the four panels. Also note that these model simulations do not include iodine emissions from ice surfaces. For the absolute values of the OSG emissions, please refer to the study of Ordóñez et al., 2012.

results, we confirm the need to include the inorganic oceanic emissions of iodine into global models and stress the need for further laboratory and theoretical studies about the atmospheric fate of I_2O_x. In particular, the model results indicate that 83 % of the total oceanic natural emissions of iodine are inorganic (mainly HOI) following the reaction of iodide with ozone at the sea surface; these inorganic emissions are indeed necessary to reproduce the observations of IO in all marine environments. Finally, our results show that the contribution of the organic/inorganic source gases to IO levels in the global MBL is geographically highly variable, existing in regions of ozone-rich outflow where the inorganic contribution to IO can be more than 90 %. This combined observational and modelling exercise strengthens the need for including both the organic and the inorganic oceanic emissions of iodine into global models for a more accurate assessment of the oxidizing capacity of the marine troposphere.

The Supplement related to this article is available online at doi:10.5194/acp-15-583-2015-supplement.

Acknowledgements. The authors would like to thank everyone involved in the Malaspina 2010 expedition, funded by the Spanish Ministry of Economy and Competitiveness. In particular the Marine Technology Unit (UTM-CSIC) for facilitating the ancillary data as well as the Hesperides *R/V* crew. We also thank Alan Thomas, John Robinson and Dave Humphries (NIWA) for building the MAX-DOAS tracker and the atmospheric group of the Institute of Environmental Physics (Heidelberg) for facilitating the gimbal table. We also thank Markus Rex for his comments on the ozone measurements during the TransBrom campaign and Klaus Pfeilsticker and John Plane for helpful discussions. The Indian Institute of Tropical Meteorology is supported by the Ministry of Earth Sciences, Government of India. R. P. Fernandez would like to thank ANPCyT (PICT-PRH 2009-0063) for financial support.

Edited by: A. Pszenny

References

Barrie, L. A., Bottenheim, J. W., Schnell, R. C., Crutzen, P. J., and Rasmussen, R. A.: Ozone depletion and photochemical reactions at polar sunrise in the lower Arctic atmosphere, Nature, 334, 138–141, 1988.

Bell, N., Hsu, L., Jacob, D. J., Schultz, M. G., Blake, D. R., Butler, J. H., King, D. B., Lobert, J. M., and Maier-Reimer, E.: Methyl iodide: Atmospheric budget and use as a tracer of marine convection in global models, J. Geophys. Res. Atmos., 107, 4340, doi:10.1029/2001JD001151, 2002.

Carpenter, L. J., Archer, S. D., and Beale, R.: Ocean-atmosphere trace gas exchange, Chem. Soc. Rev., 41, 6473–6506, doi:10.1039/C2CS35121H, 2012.

Carpenter, L. J., MacDonald, S. M., Shaw, M. D., Kumar, R., Saunders, R. W., Parthipan, R., Wilson, J., and Plane, J. M. C.: Atmospheric iodine levels influenced by sea surface emissions of inorganic iodine, Nature Geosci., 6, 108–111, 2013.

Chameides, W. L. and Davis, D. D.: Iodine: Its possible role in tropospheric photochemistry, J. Geophys. Res., 85, 7383–7398, 1980.

Dix, B., Baidar, S., Bresch, J. F., Hall, S. R., Schmidt, K. S., Wang, S., and Volkamer, R.: Detection of iodine monoxide in the tropical free troposphere, P. Natl. Acad. Sci., 110, 2035–2040, 2013.

Draxler, R. R. and Rolph, G. D.: HYSPLIT (HYbrid Single-Particle Lagrangian Integrated Trajectory) Model access via NOAA ARL READY Website http://ready.arl.noaa.gov/HYSPLIT.php (last access: 20 May 2014), NOAA Air Resources Laboratory, Silver Spring, MD, 2014.

Garland, J. A., Elzerman, A. W., and Penkett, S. A.: The Mechanism for Dry Deposition of Ozone to Seawater Surfaces, J. Geophys. Res., 85, 7488–7492, 1980.

Gómez Martín, J. C., Mahajan, A. S., Hay, T. D., Prados-Román, C., Ordóñez, C., MacDonald, S. M., Plane, J. M. C., Sorribas, M., Gil, M., Paredes Mora, J. F., Agama Reyes, M. V., Oram, D. E., Leedham, E., and Saiz-Lopez, A.: Iodine chemistry in the eastern Pacific marine boundary layer, J. Geophys. Res. Atmos., 118, 887–904, doi:10.1002/jgrd.50132, 2013a.

Gómez Martín, J. C., Gálvez, O., Baeza-Romero, M. T., Ingham, T., Plane, J. M. C., and Blitz, M. A.: On the mechanism of iodine oxide particle formation, Phys. Chem. Chem. Phys., 15, 15612–15622, doi:10.1039/C3CP51217G, 2013b.

Großmann, K., Frieß, U., Peters, E., Wittrock, F., Lampel, J., Yilmaz, S., Tschritter, J., Sommariva, R., von Glasow, R., Quack, B., Krüger, K., Pfeilsticker, K., and Platt, U.: Iodine monoxide in the Western Pacific marine boundary layer, Atmos. Chem. Phys., 13, 3363–3378, doi:10.5194/acp-13-3363-2013, 2013.

Hönninger, G., Friedeburg, C. V., and Platt, U.: Multi axis differential optical absorption spectroscopy (MAX-DOAS), Atmos. Chem. Phys., 4, 231–254, doi:10.5194/acp-4-231-2004, 2004.

Jones, A. E., Anderson, P. S., Wolff, E. W., Roscoe, H. K., Marshall, G. J., Richter, A., Brough, N., and Colwell, S. R.: Vertical structure of Antarctic tropospheric ozone depletion events: characteristics and broader implications, Atmos. Chem. Phys., 10, 7775–7794, doi:10.5194/acp-10-7775-2010, 2010.

Lamarque, J. F., Emmons, L. K., Hess, P. G., Kinnison, D. E., Tilmes, S., Vitt, F., Heald, C. L., Holland, E. A., Lauritzen, P. H., Neu, J., Orlando, J. J., Rasch, P. J., and Tyndall, G. K.: CAM-chem: description and evaluation of interactive atmospheric chemistry in the Community Earth System Model, Geosci. Model Dev., 5, 369–411, doi:10.5194/gmd-5-369-2012, 2012.

Lawler, M. J., Mahajan, A. S., Saiz-Lopez, A., and Saltzman, E. S.: Observations of I_2 at a remote marine site, Atmos. Chem. Phys., 14, 2669–2678, doi:10.5194/acp-14-2669-2014, 2014.

MacDonald, S. M., Gómez Martín, J. C., Chance, R., Warriner, S., Saiz-Lopez, A., Carpenter, L. J., and Plane, J. M. C.: A laboratory characterisation of inorganic iodine emissions from the sea surface: dependence on oceanic variables and parameterisation for global modelling, Atmos. Chem. Phys., 14, 5841–5852, doi:10.5194/acp-14-5841-2014, 2014.

Mahajan, A. S., Plane, J. M. C., Oetjen, H., Mendes, L., Saunders, R. W., Saiz-Lopez, A., Jones, C. E., Carpenter, L. J., and McFig-

gans, G. B.: Measurement and modelling of tropospheric reactive halogen species over the tropical Atlantic Ocean, Atmos. Chem. Phys., 10, 4611–4624, doi:10.5194/acp-10-4611-2010, 2010.

Mahajan, A. S., Gómez Martín, J. C., Hay, T. D., Royer, S. J., Yvon-Lewis, S., Liu, Y., Hu, L., Prados-Roman, C., Ordóñez, C., Plane, J. M. C., and Saiz-Lopez, A.: Latitudinal distribution of reactive iodine in the Eastern Pacific and its link to open ocean sources, Atmos. Chem. Phys., 12, 11609–11617, doi:10.5194/acp-12-11609-2012, 2012.

Molina, M. J. and Rowland, F. S.: Stratospheric sink for chlorofluoromethanes: Chlorine-atom catalysed destruction of ozone, Nature, 249, 810–812, 1974.

Myhre, G., D. Shindell, D., Bréon, F.-M., Collins, W., Fuglestvedt, J., Huang, J., Koch, D., Lamarque, J.-F., Lee, D., Mendoza, B., Nakajima, T., Robock, A., Stephens, G., Takemura, T. and Zhang, H.: Anthropogenic and Natural Radiative Forcing. In: Climate Change 2013: The Physical Science Basis. Contribution of Working Group I to the Fifth Assessment Report of the Intergovernmental Panel on Climate Change edited by: Stocker, T. F., Qin, D., Plattner, G.-K., Tignor, M., Allen, S. K., Boschung, J., Nauels, A., Xia, Y., Bex, V., and Midgley, P. M., Cambridge University Press, Cambridge, UK and New York, NY, USA, Chap. 8, 670–688, 2013.

Ordóñez, C., Lamarque, J. F., Tilmes, S., Kinnison, D. E., Atlas, E. L., Blake, D. R., Sousa Santos, G., Brasseur, G., and Saiz-Lopez, A.: Bromine and iodine chemistry in a global chemistry-climate model: description and evaluation of very short-lived oceanic sources, Atmos. Chem. Phys., 12, 1423–1447, doi:10.5194/acp-12-1423-2012, 2012.

Platt, U. and Stutz, J.: Differential Absorption Spectroscopy, in: Differential Optical Absorption Spectroscopy, Physics of Earth and Space Environments, Springer, Berlin Heidelberg, 135–174, 2008.

Prados-Roman, C., Cuevas, C. A., Fernandez, R. P., Kinnison, D. E., Lamarque, J.-F., and Saiz-Lopez, A.: A negative feedback between anthropogenic ozone pollution and enhanced ocean emissions of iodine, Atmos. Chem. Phys. Discuss., 14, 21917–21942, doi:10.5194/acpd-14-21917-2014, 2014.

Rayner, N. A., Parker, D. E., Horton, E. B., Folland, C. K., Alexander, L. V., Rowell, D. P., Kent, E. C., and Kaplan, A.: Global analyses of sea surface temperature, sea ice, and night marine air temperature since the late nineteenth century, J. Geophys. Res. Atmos., 108, 4407, doi:10.1029/2002JD002670, 2003.

Read, K. A., Mahajan, A. S., Carpenter, L. J., Evans, M. J., Faria, B. V. E., Heard, D. E., Hopkins, J. R., Lee, J. D., Moller, S. J., Lewis, A. C., Mendes, L., McQuaid, J. B., Oetjen, H., Saiz-Lopez, A., Pilling, M. J., and Plane, J. M. C.: Extensive halogen-mediated ozone destruction over the tropical Atlantic Ocean, Nature, 453, 1232–1235, 2008.

Saiz-Lopez, A. and von Glasow, R.: Reactive halogen chemistry in the troposphere, Chem. Soc. Rev., 41, 6448–6472, doi:10.1039/C2CS35208G, 2012.

Saiz-Lopez, A., Plane, J. M. C., Mahajan, A. S., Anderson, P. S., Bauguitte, S. J.-B., Jones, A. E., Roscoe, H. K., Salmon, R. A., Bloss, W. J., Lee, J. D., and Heard, D. E.: On the vertical distribution of boundary layer halogens over coastal Antarctica: implications for O_3, HO_x, NO_x and the Hg lifetime, Atmos. Chem. Phys., 8, 887–900, doi:10.5194/acp-8-887-2008, 2008.

Saiz-Lopez, A., Plane, J. M. C., Baker, A. R., Carpenter, L. J., Von Glasow, R., Gómez Martín, J. C., McFiggans, G., and Saunders, R. W.: Atmospheric Chemistry of Iodine, Chem. Rev., 112, 1773–1804, doi:10.1021/cr200029u, 2012.

Saiz-Lopez, A., Fernandez, R. P., Ordóñez, C., Kinnison, D. E., Gómez Martín, J. C., Lamarque, J.-F., and Tilmes, S.: Iodine chemistry in the troposphere and its effect on ozone, Atmos. Chem. Phys., 14, 13119–13143, doi:10.5194/acp-14-13119-2014, 2014.

Wagner, T., Dix, B., Friedeburg, C. v., Frieß, U., Sanghavi, S., Sinreich, R., and Platt, U.: MAX-DOAS O_4 measurements: A new technique to derive information on atmospheric aerosols – Principles and information content, J. Geophys. Res. Atmos., 109, D22205, doi:10.1029/2004JD004904, 2004.